Proceedings of the Combustion Institute 40 (2024) 105457

Contents lists available at ScienceDirect

Proceedings of the Combustion Institute

journal homepage: www.elsevier.com/locate/proci

Rotational-vibrational O_2–CO_2 coherent anti-Stokes Raman spectroscopy for determination of thermochemical states in oxy-fuel biomass combustion

Henrik Schneider [a,*], Janik Hebel [a], Benjamin Böhm [a], Reinhold Kneer [b], Andreas Dreizler [a]

[a] Technical University of Darmstadt, Department of Mechanical Engineering, Reactive Flows and Diagnostics, Otto-Berndt-Str. 3, Darmstadt 64287, Germany
[b] RWTH Aachen University, Faculty of Mechanical Engineering, Institute of Heat and Mass Transfer, Augustinerbach 6, Aachen 52062, Germany

ARTICLE INFO

Keywords:
Laser diagnostics
CARS
Oxy-fuel combustion
Thermochemical state
Biomass combustion

ABSTRACT

This study focuses on the development and application of an in-situ and non-intrusive measurement technique to determine the thermochemical states in pulverized oxy-fuel combustion in the absence of N_2. This is a challenging task in such harsh environments and has not been achieved for oxy-fuel combustion. Coherent anti-Stokes Raman spectroscopy (CARS) using the probe molecules O_2 and CO_2 was chosen to access the thermochemical states in all flame regions. Experimental validation of the developed O_2-CO_2-CARS setup showed relative accuracies below 3% and relative precisions around 5% for the determination of gas temperatures up to 2100 K. The mole fractions of O_2 and CO_2 could be estimated with relative accuracies below 6% when both species were present in the gas mixture with mole fractions greater than 0.2. For small amounts of O_2, CO_2 mole fractions showed relative accuracies around 5% and relative precisions around 10%. The O_2-CO_2-CARS setup was applied to a solid fuel combustor operating swirled gas-assisted pulverized fuel flames under oxy-fuel conditions up to 70 kW_{th}. First, the gas flame was investigated solely, showing maximum temperatures close to the maximum adiabatic flame temperatures and consistency with the flow field investigated in a previous study. The subsequent investigation of gas-assisted pulverized fuel combustion using walnut shell particles as a biomass representative demonstrated the applicability of the developed O_2-CO_2-CARS setup in particle-laden reactive flows. A strong influence of the solid fuel particles on the inner recirculation zone of the swirl flame was observed. The thermochemical state within the inner recirculation zone was found to be almost spatially homogeneous, while broad distributions were found within the mixing zone of the main flow and the outer recirculation zone. In this region a linear relationship between O_2 mole fractions and gas temperature was observed with decreasing O_2 mole fractions with increasing temperature.

1. Introduction

Oxy-fuel combustion of pulverized solid fuel is a promising approach to produce CO_2–rich flue gases for the efficient application of carbon capture and storage or usage (CCS/CCU) technologies. This process involves the combustion of solid fuel in an atmosphere composed mainly of O_2, CO_2 and H_2O. This is achieved by recirculating part of the flue gas and introducing solid fuel and oxygen, previously separated from the atmospheric air.

For an improved understanding of the underlying physicochemical processes in pulverized oxy-fuel combustion, knowledge of the thermochemical states is valuable as it provides insight into the reaction transport manifolds of combustion processes. However, this is a challenging task in harsh environments such as solid fuel combustion.

To assess the mole fractions of educt and product gases within the combustion process, ex-situ gas sampling techniques are typically used (e.g. [1]), while gas temperatures in pulverized fuel combustion are usually measured using suction pyrometers [2,3]. For non-intrusive determination of gas temperatures, laser diagnostics such as tomographic absorption spectroscopy have been used [4].

Coherent anti-Stokes Raman spectroscopy (CARS) as a non-intrusive laser optical method allows the simultaneous measurement of gas temperature and mole fractions of major educt or product species. Hughes et al. [2] compared ex-situ suction pyrometry with in-situ temperature measurements by CARS and found that CARS-derived temperatures were more reliable. Demonstrations of CARS measurements in pulverized coal combustion have also been performed by Eckbreth [5], Aldén et al. [6], and Beiting [7]. However, they used N_2 as the probe molecule to derive gas temperatures which is not present in oxy-fuel combustion. Tröger et al. [8] developed a high temperature O_2 vibrational CARS setup for thermometry in oxy-fuel combustion, which was applied

* Corresponding author.
E-mail address: hschneider@rsm.tu-darmstadt.de (H. Schneider).

https://doi.org/10.1016/j.proci.2024.105457
Received 28 November 2023; Accepted 17 June 2024
Available online 23 July 2024

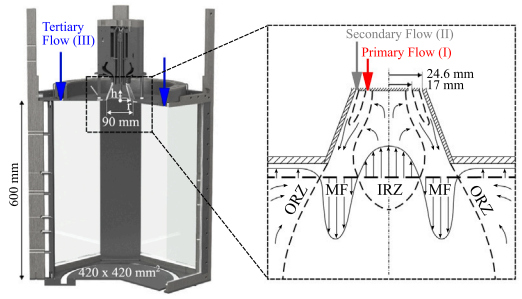

Fig. 1. Solid Fuel Combustor (SFC) including flow field in the near-nozzle region based on previous investigations with particle image velocimetry (PIV) [12]. IRZ: Inner recirculation zone. MF: Main flow downwards. ORZ: Outer recirculation zone.

to the combustor investigated in this study by Meißner et al. [9]. They obtained good results in regions where local O_2 concentrations are sufficiently high, while no measurements were possible in regions where O_2 concentrations were low.

Recently, Mazza et al. [10] developed an ultra-broadband two-beam femtosecond/picosecond rotational-vibrational O_2–CO_2–CARS approach for simultaneous thermometry and relative O_2/CO_2 concentration measurements for high temperature applications. This approach is targeted at oxy-fuel and moderate or intense low oxygen dilution (MILD) combustion applications and has demonstrated high accuracy.

In the present study, a nanosecond rotational-vibrational O_2–CO_2–CARS setup is developed and applied to a solid fuel combustor to determine thermochemical states in oxy-fuel biomass combustion. The novel O_2–CO_2–CARS approach is thoroughly quantified in terms of accuracy and precision with measurements above a flat flame by comparison with equilibrium calculations. Spectra evaluation is performed using the "carsfwsc" algorithm of Cutler et al. [11].

2. Methods

2.1. Solid fuel combustor

The Solid Fuel Combustor (SFC) was designed to mimic close-to-reality conditions within the near-nozzle region of pulverized solid fuel combustion chambers (Fig. 1). The SFC operates swirled, gas-assisted pulverized solid fuel flames up to 70 kW_{th} under oxy-fuel atmospheres and provides large optical access through quartz glass walls for laser-optical diagnostics.

Three flows enter the SFC, the primary (I) and secondary (II) flows issue through orifices in the burner, while the tertiary flow (III) enters through the top of the combustion chamber. The I flow consists of partially premixed fuel, including solid fuel particles, while the II and III flows consist of O_2 and CO_2. The operation conditions studied include a single-phase case (methane combustion), designated OXY33P, and a two-phase case (gas-assisted solid fuel combustion), denoted OXY33P-WS (Table 1). They represent a subset of a wider range of operation conditions [12]. As pulverized solid fuel, walnut shell (WS) particles in the size range between 100 µm (D10) and 180 µm (D90) were used as a biomass representative. Further analyses of the WS particles are given in [12].

2.2. Coherent anti-Stokes Raman spectroscopy

A combined O_2-CO_2-CARS approach was used to determine the thermochemical states under oxy-fuel conditions.

The laser wavelengths were chosen to be 561.5 nm, 612.3 nm, and 532 nm for the pump, Stokes, and probe lasers, respectively, similar to the work of Lucht [15], Lucht et al. [16], Roy et al. [17], and Zentgraf et al. [18]. Since the Stokes laser was spectrally broadband, this results in the detection of all Raman active transitions

Table 1
SFC operation conditions. Values in brackets belong to OXY33P-WS.

Operation condition		OXY33P(-WS)
Oxidizer: O_2/CO_2	vol.%	33/67
I Methane	m^3_n/h	3.17
I Particle mass flow	kg/h	(6.02)
I Oxidizer	m^3_n/h	12.10
II Oxidizer	m^3_n/h	11.09
III Oxidizer	m^3_n/h	24.02
Thermal power	kW_{th}	31.5 (63)
Local stoich. ratio (I+II)	–	1.21 (0.61)
Global stoich. ratio (I+II+III)	–	2.47 (1.25)
Swirl number	–	0.43
$T_{ad,max}$ [a]	K	2272

[a] T_{ad} is calculated with Cantera [13] and the GRI 3.0 mechanism [14] and is maximal at an equivalence ratio of 1.08.

around ω_R = 1478 cm^{-1}, which includes the Q-branch transitions of O_2 around a Raman shift of 1556 cm^{-1} and the $2\upsilon_2$ system of CO_2 around 1388 cm^{-1}. The experimental setup also allows the detection of the Q-branch transitions of N_2 around a Raman shift of 2330 cm^{-1}, which is achieved by a dual-pump CARS approach. Due to the oxy-fuel conditions, N_2 is not present in the spectra measured in this paper.

A Q-switched, frequency-doubled Nd:YAG laser with two Nd:YAG cavities (Spectra-Physics PIV 400, 10 Hz, 5 −8 ns pulse width) was modified for individual operation of both cavities. One cavity was used to optically pump a narrowband dye laser (Radiant Dyes Laser & Accessories GmbH, NarrowScan) to generate the pump laser beam at 561.5 nm. Rhodamine 590 dye dissolved in ethanol was used as the lasing medium. The laser from the other cavity was split into two paths, one serving as the probe beam at 532 nm and one to optically pump a custom-built broadband dye laser to produce the Stokes laser beam around 612 nm.

The modeless broadband dye laser consisted of a transversally pumped oscillator followed by two longitudinally pumped amplifier stages. The dye Rhodamine 640 dissolved in ethanol was used as the lasing medium to produce spectrally broadband laser radiation with a center wavelength of 612.3 nm and a full width at half maximum (FWHM) of approx. 5 nm.

All lasers were energy controlled by a combination of a zero-order half-wave plate and a polarizing beamsplitter cube. Beam divergences were adjusted by two lenses in each beam path. To synchronize the temporal overlay of Stokes and probe beams, a delay line was constructed within the beam path of the probe laser. The timing of the pump beam with respect to the probe and Stokes lasers was adjusted by the Q-switch delay. The temporal resolution was calculated as the $1/e^2$-value of the convolved intensity of the normalized individual temporal intensity profiles to 8.1 ns with a standard deviation of 0.45 ns.

The laser beams were focused to the probe volume by a spherical lens with a focal length of f = 300 mm. Phase matching was achieved by a planar BOXCARS arrangement to allow measurements close to the combustor dump plane. The angles were set to $\alpha \approx -2°$, $\beta \approx 2.2°$, and $\gamma \approx 1.9°$ with respect to the optical axis for pump, Stokes, and probe beams, respectively. The size of the probe volume was determined by traversing a beam monitor (DataRay Inc., WinCam D) in increments of 0.5 mm along the optical axis in the vicinity of the probe volume. The size of the CARS probe was derived as the $1/e^2$-value of the normalized convolved intensity to an elliptical area at the center with a minor axis of $a \approx 40$ µm and a major axis of $b \approx 50$ µm. The length of the probe volume was calculated by interpolating the normalized convolved intensity to $l \approx 0.7$ mm.

The CARS signal was collimated with a spherical lens of the same focal length as the focusing lens (f = 300 mm). Due to the applied phase matching scheme, the CARS signal was spatially close to the

pump beam. Separation of the pump and CARS beams and suppression of flame luminosity was performed by three short pass dichroic mirrors (Thorlabs Inc., DMLP550L) and a short pass filter (Thorlabs Inc., FESH0550). Additionally, a notch filter removed scattered radiation at 532 nm. A motorized filter wheel with different neutral density (ND) filters, ranging from ND0 (no filter) to ND2.9, was positioned in the beam path to account for local variations in signal strength due to changes in temperature and mole fraction. To optimize the polarization of the CARS signal with respect to the spectrometer, an achromatic half-wave plate was placed in the beam path. Subsequently, the CARS signal was focused into the entrance slit of a spectrometer (Jobin Yvon S.A.S., THR 1000 Monochromator, focal length 1 m, 2400 lines/mm grating) by a spherical lens with a focal length of $f = 100$ mm. The chip of a back-illuminated CCD camera (Princeton Instruments, Pixis 400B, 1340 x 400 px, 16 bit) was placed at the position of the exit slit to record the CARS spectra. The chip was fully hardware binned in the vertical direction and the camera frame rate was set to 20 Hz, twice the laser repetition rate to record background spectra between the CARS spectra.

In order to normalize the CARS spectra to the spectral profile of the broadband Stokes laser, non-resonant spectra were recorded several times during the measurements in pure argon.

The pulse energies of the pump, Stokes, and probe lasers within the probe volume were set to 25 mJ, 23.5 mJ, and 30 mJ. To check for high irradiance perturbation effects, the laser energies were varied and CARS spectra above a flat flame, operated under oxy-fuel conditions with 20 vol.% O_2 in the flue gas, were recorded. The laser energy variation did not show any significant changes in the spectra, proving that the selected laser energies did not lead to high irradiance perturbation effects [19]. Mean spectra of the laser energy variation are provided in Fig. S1, available in the supplementary material.

2.3. Data processing

2.3.1. Pre-processing of CARS spectra

The pre-processing of the CARS spectra involved preparing the spectra to be processed using the "carsfwsc" algorithm of Cutler et al. [11]. Special algorithms were required to remove spectra suffering from saturation, low signal-to-noise ratios, or laser-induced breakdowns. Optical breakdowns occurred when particles were inside the probe volume and were hit by the lasers, which is inevitable in pulverized fuel combustion.

Saturation of the spectra was detected at a threshold of 65 000 counts and occurred most frequently at positions where cold oxidizer and hot exhaust gases mix. At all other positions, saturation was successfully prevented by a suitable choice of ND filter in front of the spectrometer. To avoid a bias at positions with saturated spectra, the same position was measured again using an ND filter with a higher optical density. In post-processing, the two datasets were merged by appending the n spectra with the highest intensity counts from the dataset recorded with the ND filter with the higher optical density to the first dataset where n spectra experienced saturation.

Spectra with low signal-to-noise ratios were removed when the intensity of the peak signal was less than six times the standard deviation of the spectra. This criterion was chosen to avoid dependence of the signal-to-noise ratio on the measurement results. For the single-phase operation condition OXY33P 0.7% of all recorded spectra and for the gas-assisted solid fuel condition OXY33P-WS 5.9% of all recorded spectra were removed due to too low signal-to-noise ratios.

Laser-induced breakdowns led to a deformation of the recorded spectra. Most spectra affected by optical breakdown showed a strong overall increase in intensity. These spectra could be easily removed by applying a threshold to the sum of the intensities in a spectral region where no transitions were expected. However, there were also smaller, spectrally confined distortions that were removed by detecting artificially high intensity values in regions where no Raman active transitions exist.

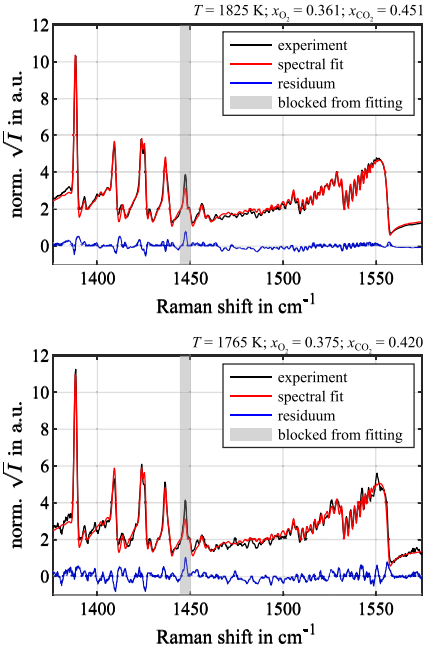

Fig. 2. Experimental and fitted CARS spectra. Top: Mean O_2–CO_2–CARS spectra. Bottom: Instantaneous O_2–CO_2–CARS spectra.

For single-phase operation conditions almost no laser induced breakdowns were detected, whereas for pulverized solid fuel combustion the number of optical breakdowns was highly dependent on the measurement position. Analyses are given in the results section.

All good spectra underwent further pre-processing. First, the background intensity was subtracted from the recorded CARS spectra. In the case of single-phase operation conditions, an average background signal was calculated and then subtracted from each CARS spectrum. However, this approach was not feasible for the two-phase operation conditions due to the high intensity fluctuations of the background signal. Therefore, the mean background signal was weighted by the mean intensity value of a spectral band where no Raman transitions were expected. A justification for this approach is provided in Fig. S2, available in the supplementary material. Background signals and CARS signals almost coincide on one line when normalized by area, meaning that background signals can be scaled in a frequency independent way.

The recorded CARS spectra were normalized to the non-resonant spectrum measured in pure argon. The non-resonant spectrum was interpolated in time using non-resonant spectra recorded before and after the measurement. Spectra were only processed if the non-resonant signals taken in pure argon deviated very little from time to time. This was tested by fitting the CARS spectra with the non-resonant signals before and after the data series. CARS spectra were discarded if the temperature difference exceeded 30 K.

Finally, the square root of the intensity was extracted and the pixel to wavenumber conversion was performed. The wavenumber axis related to the dispersion of the spectrometer was calibrated using a measured spectrum above a flat flame and a simulated spectrum of the same conditions. The spectrum was simulated using the "carsfwsc" algorithm. A second order polynomial fit of all transition peaks was performed to convert pixels to wavenumbers using a least square method. While linear fits were successfully applied for small spectral fit windows, non-linear behavior is evident for large spectral fit windows [19].

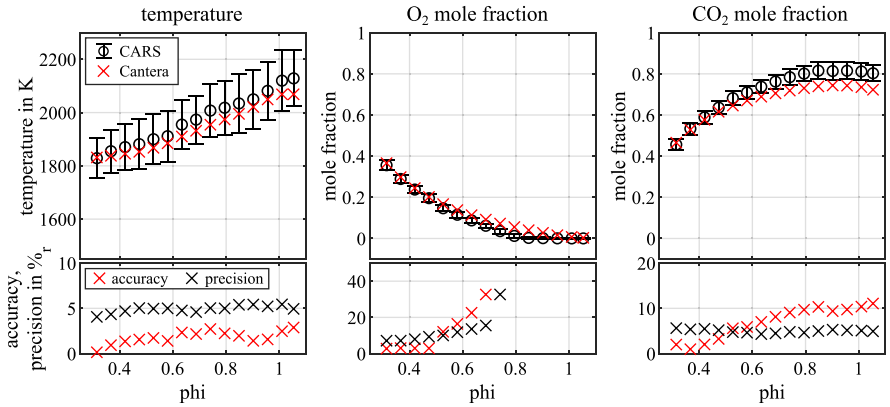

Fig. 3. Relative accuracies and precisions of the O_2–CO_2–CARS setup for different equivalence ratios.

2.3.2. CARS spectra fitting

CARS spectra were fitted using the "carsfwsc" algorithm of Cutler et al. [11], which is based on CARSFT [20] with improved models of the Herman Wallis factor based on Marrocco et al. [21].

The bounds for the fit variables were set wide to avoid any influence of the bounds on the precision of the measurement. O_2 and CO_2 Raman transitions with Raman shifts between 1372 cm^{-1} to 1572 cm^{-1} were fitted. The range 1444.5 cm^{-1} to 1450.5 cm^{-1} had to be blocked from fitting, since the Raman active rotational line S(5) of H_2 at 1447.28 cm^{-1} [22] affected the measured spectra and could not be resolved properly by the "carsfwsc" algorithm. The third order non-resonant susceptibility χ_{NR} was set to $19.74 \cdot 10^{-18}$ cm^3/(erg amagat) [23] as it was assumed that H_2O makes up the majority of the buffer gas.

Examples of measured and fitted spectra are shown in Fig. 2. Both mean and instantaneous spectra were well fitted with the described parameters, resulting in a low residuum.

3. Results and discussion

3.1. Experimental validation

The experimental validation of O_2–CO_2–CARS was performed to determine the accuracy and precision of the experimental setup in combination with the "carsfwsc" algorithm of Cutler et al. [11].

Measurements were conducted in the exhaust of a premixed flat flame and compared with reference values calculated with Cantera [13] in combination with the GRI 3.0 mechanism [14]. The flat flame was stabilized over a ceramic honeycomb structure with a square cross-section of 76.2 × 76.2 mm^2 and a cross-section of each channel of 1.07 × 1.07 mm^2 with a length of 50 mm. Various gas mixtures of $CH_4/O_2/CO_2$ were premixed and issued from the ceramic honeycomb structure.

O_2–CO_2–CARS spectra were recorded approx. 10 mm above the flat flame for flames with different equivalence ratios. For each operation condition, 500 individual O_2–CO_2–CARS spectra were evaluated. For the thermal equilibrium calculations, a preheated gas temperature of 70 °C was used, approximated from thermocouple measurements inside one selected channel of the ceramic honeycomb structure close to its exit. The results of the measurements together with the calculated values are presented in Fig. 3. In addition, the relative accuracies and relative precisions for the gas temperature and the mole fractions of O_2 and CO_2 are depicted.

The experimental validation shows that the relative accuracy for the gas phase temperature is below 3% and the relative precision is around 5%. While the relative precision is almost constant over the temperature range considered, the relative accuracy decreases slightly with increasing temperature. This is probable due to the decreasing mole fraction of O_2 at equivalence ratios closer to 1. Similar accuracies and precisions have been reported from an N_2–CO_2 dual-pump CARS setup [18] and from the study by Mazza et al. [10] using an ultra-broadband two-beam femtosecond/picosecond O_2–CO_2–CARS approach.

O_2 and CO_2 mole fractions show relative accuracies below 6% when both species are present in the gas mixture with mole fractions greater than 0.2. For operation conditions with low O_2 concentrations in the flue gas of the flat flame, the relative accuracies decrease significantly for O_2 mole fractions and the absolute accuracy is also worse. The reason for this is the poor signal to noise ratio in the O_2–CO_2–CARS spectra in the spectral region of the Q-branch transitions of O_2. The relative accuracy of the CO_2 mole fractions for spectra containing primary spectral features of CO_2 is about 10% while the relative precision of the CO_2 mole fractions for all operation conditions is approx. 5%.

3.2. Gas temperatures of single-phase operation condition OXY33P

CARS measurements were performed at the heights h = −24.6 mm, −49.2 mm, and −98.4 mm, with h = 0 mm corresponding to the combustor dump plane. At each height the SFC was traversed to record radial CARS spectra in steps of 3 mm in the range between r = −15 mm and 60 mm and in steps of 5 mm between r = 60 mm and 90 mm. For each position, 500 CARS spectra were recorded.

The radial mean gas temperature profiles of operation condition OXY33P (Fig. 4) show a high temperature plateau region above 2100 K in the center of the SFC with a steep temperature gradient towards an outer region of temperatures around 750 K. According to the axial velocity, the high temperature plateau region at height h = −24.6 mm is within the IRZ of the swirl flame. The steep temperature gradient is formed in the shear layer towards the ORZ, indicated by high RMS values of the axial velocity. Height h = −49.2 mm is located near the stagnation point of the flow field and height h = −98.4 mm is downstream of the IRZ.

The highest mean gas temperature of 2310 K is measured at h = −49.2 mm and r = 27 mm, which is about 150 K higher than the gas temperature in the center. In comparison with equilibrium calculations carried out with Cantera [13] (see Table 1) and given the determined accuracy, this temperature is close to the maximum adiabatic flame temperature under slightly fuel-rich conditions.

The probability density functions (PDFs) of the measurement points reveal rather narrow distributions within the IRZ, within the ORZ, and near the center downstream of the IRZ. Here, the relative standard deviations of the gas temperature are close to the relative precision of the O_2–CO_2–CARS setup, indicating locally homogeneous temperature conditions. At locations where mixing of different flows occurs, the PDFs become broad. The peaks of the PDFs show a shift towards higher temperatures than the mean temperatures on the inner side of the

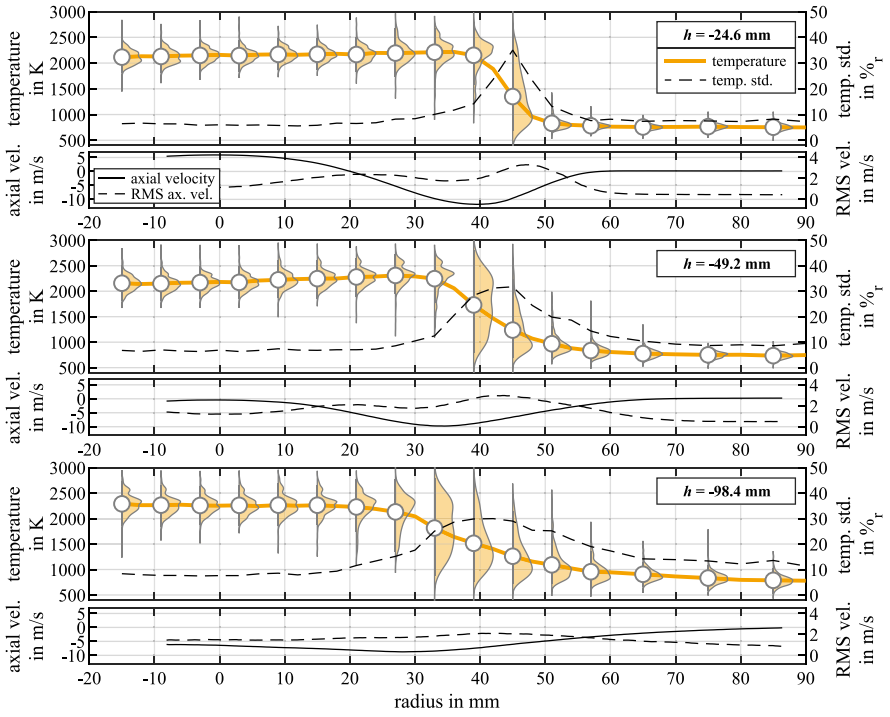

Fig. 4. Gas temperature profiles of single-phase operation condition OXY33P at the heights h = −24.6 mm, −49.2 mm, and −98.4 mm. The mean temperature is shown as solid line and the probability density function (PDF) of every second measurement point is illustrated. PDFs are multiplied by 10 for good visibility. The relative standard deviation of the gas temperature is plotted as dashed line. Axial velocity profiles and the respective RMS values are provided for comparison and are taken from [12].

region characterized by the steep temperature gradient. This contrasts with a shift towards lower temperatures than the mean temperatures of the PDF peaks at the lower end of the steep temperature gradient. These observations are typical of fluid mixing in a shear layer.

The steep temperature gradient decreases progressively in the downstream direction due to the broader shear layer. This is indicated by the radial profiles of the relative temperature standard deviation and the RMS values of the axial velocity.

Additionally, profiles of mean mole fractions of O_2 and CO_2 of the single-phase operation condition OXY33P at heights h = −24.6 mm, −49.2 mm, and −98.4 mm are provided in Fig. S3, available in the supplementary material. Note that measurements at high radial positions required the use of ND filters with high optical density values to prevent saturation caused by the strong CO_2 signals at low temperatures. This resulted in low signal-to-noise ratios in the spectral region of the Q-branch transitions of O_2. As discussed in the section of the experimental validation, this results in significantly lower accuracies in the determination of O_2 and CO_2 mole fractions, while the gas temperature evaluation is satisfactory. The erroneous O_2 and CO_2 mole fractions were removed during post-processing based on signal-to-noise ratios within the spectral range of the Q-branch transitions of O_2.

3.3. Thermochemical state of gas-assisted pulverized fuel combustion in oxy-fuel

CARS measurements for the two-phase operation condition OXY33P-WS were performed at every second measurement position of the OXY33P grid. For each position, 600 to 1000 CARS spectra were recorded to account for spectra containing laser-induced breakdowns. This ensured that at least 300 spectra were processed for each position, while most positions had 500 to 600 spectra that could be evaluated.

Radial mean gas temperature profiles are shown in Fig. 5 for the heights h = −24.6 mm, −49.2 mm, and −98.4 mm along with the respective fraction of good spectra at each measurement position. Spectra removed during processing and classified as ‘not good’ suffered mainly from laser-induced breakdowns, while saturation or low signal-to-noise ratios played a minor role.

The radial mean gas temperature profile at h = −24.6 mm exhibits a temperature drop to about 1700 K within the IRZ. Within the zone of the main flow downwards, surrounding the IRZ, the gas temperature rises and is at the same level as the gas temperature of the single-phase operation condition OXY33P. The fraction of good spectra is reduced by laser-induced breakdown due to particles within the probe volume, mostly within a radius of 20 mm around the center. In this region, 20% to 35% of all recorded spectra suffered from breakdown. These observations suggest that the IRZ is predominantly influenced by the solid fuel particles, which heat up and release volatiles into an environment with a low O_2 concentration. In contrast, the main flow downwards is dominated by methane and volatile combustion.

The temperature gradient towards the ORZ is flattened for gas-assisted solid fuel combustion compared to single-phase combustion, and the temperature level within the ORZ is about 250 K higher, caused by the increase in total thermal power.

Further downstream, at heights h = −49.2 mm and h = −98.4 mm, the gas temperature of the central zone is between 1500 K and 2000 K. The highest radial gas temperatures are obtained at the radial position of about r = 40 mm. In contrast to OXY33P, the steep temperature gradient towards the ORZ is expanded radially outward, flattened, and obtains a reduced absolute temperature difference.

The gas temperature distribution of the individual measurements is similar to that of the single-phase operation condition OXY33P and is further examined in the O_2–T, CO_2–T, and O_2–CO_2 state spaces (Fig. 6). Additionally, profiles of mean mole fractions of O_2 and CO_2 of the two-phase operation condition OXY33P-WS at heights h = −24.6 mm, −49.2 mm, and −98.4 mm are provided in Fig. S4, available in the supplementary material.

The state spaces are analyzed for a position within the IRZ (h = −24.6 mm, r = 3 mm) and a position within the mixing zone (h = −49.2 mm, r = 45 mm).

The location within the IRZ exhibits a narrow distribution of individual measurements with a mean gas temperature of 1720 K (relative

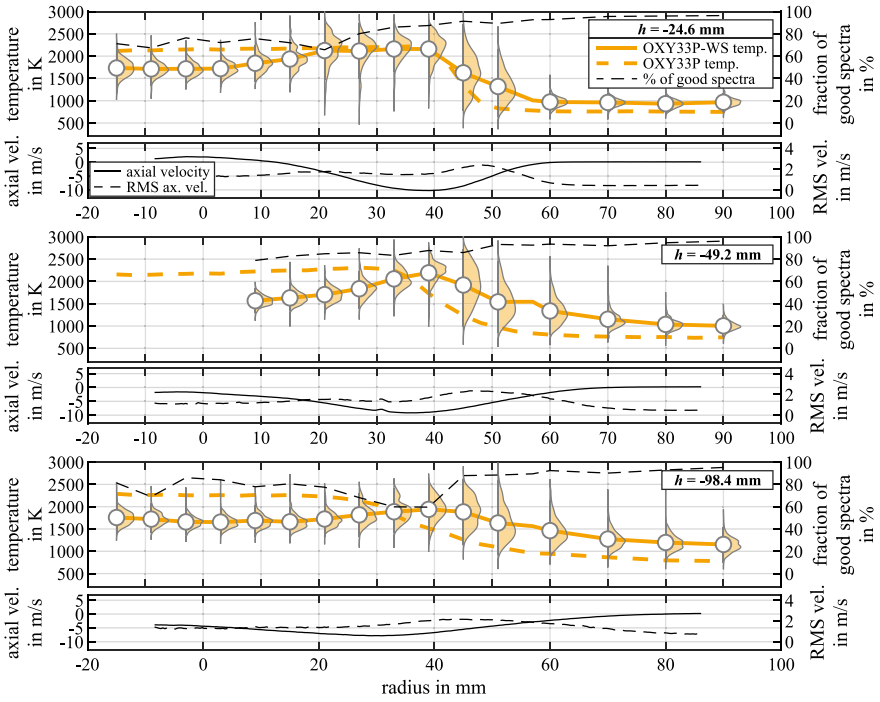

Fig. 5. Gas temperature profiles of the two-phase operation condition OXY33P-WS at heights h = —24.6 mm, —49.2 mm, and —98.4 mm. The mean temperature is shown as a solid line and the PDF is presented. PDFs are multiplied by 10 for good visibility. The mean gas temperature of OXY33P is depicted for comparison. The fraction of evaluated good spectra is shown as a black dashed line. Measurements in the center at h = —49.2 mm have been removed due to low signal-to-noise ratios.

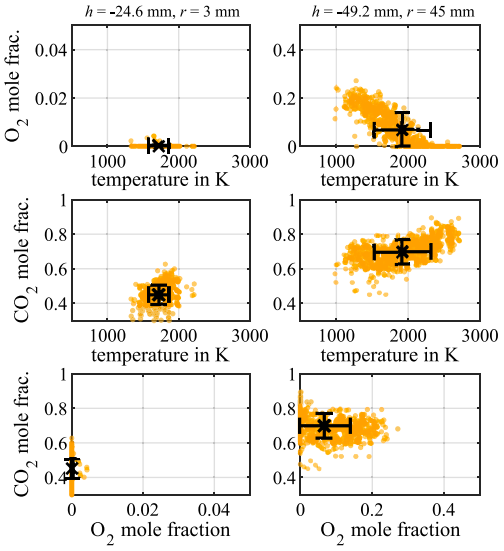

Fig. 6. Thermochemical state for two locations of the two-phase operation condition OXY33P-WS. Left column: Location: h = —24.6 mm, r = 3 mm. Right column: Location: h = —49.2 mm, r = 45 mm.

standard deviation: 8%), an O_2 mole fraction close to 0, and a mean CO_2 mole fraction of 0.45 (relative standard deviation: 12%). Compared to the measurement precision, the relative standard deviations are only slightly larger, indicating almost spatially homogeneous thermochemical states in the center of the IRZ. Note that the accuracy of the CO_2 and O_2 mole fractions in the center of the flame is lower because the buffer gas is assumed to consist only of H_2O, ignoring contributions from H_2, CO, and other fuel species.

The O_2-T state space in the mixing zone of OXY33P-WS reveals a linear relationship between gas temperature and O_2 mole fraction, with decreasing O_2 mole fractions with increasing temperature. The individual measurements are evenly distributed over the entire temperature range, indicating the presence of all thermochemical states between the high temperature plateau region of the IRZ and the thermochemical state of the ORZ. The CO_2–T and O_2–CO_2 state spaces exhibit no clear correlations, while the distribution of individual measurements is broad.

4. Conclusion

This study presents a comprehensive analysis of the thermochemical states of oxy-fuel combustion in the near-nozzle region of a gas-assisted solid fuel combustor for single-phase and two-phase reactive flows. To achieve this, a novel O_2–CO_2–CARS approach was successfully implemented and experimentally validated using a flat flame and equilibrium calculations performed with Cantera [13] for high temperatures. The results show high relative accuracies (below 3%) and high relative precisions (~5%) for hot gas temperature evaluations. Mole fractions of O_2 and CO_2 are well estimated (rel. accuracy below 6%) when both species are present in the gas mixture with mole fractions greater than 0.2. CO_2 mole fractions for smaller amounts of O_2 exhibit relative accuracies about 10%. The relative precision of CO_2 mole fractions is approx. 5% for the oxy-fuel atmospheres studied.

The main findings of the analysis of the thermochemical states of single-phase and two-phase combustion are summarized as follows:

- For both single-phase and two-phase operation conditions, the thermochemical states within the IRZ are almost spatially homogeneous.
- The single-phase operation conditions show gas temperatures close to the respective maximum adiabatic flame temperatures within the main flow downwards, which surrounds the IRZ.
- In gas-assisted solid fuel combustion, the IRZ is predominantly influenced by the solid fuel particles, which experience heat up and release volatiles, while the main flow downwards is dominated by the combustion of methane and volatiles.

- A linear relationship between O_2 mole fractions and gas temperature within the mixing zone of the main flow downwards and the ORZ is observed.

Novelty and Significance Statement

In this study, a novel O2-CO2-CARS approach was developed and characterized in terms of accuracy and precision. The subsequent stepwise application to oxy-fuel methane combustion and gas-assisted pulverized biomass combustion under oxy-fuel atmospheres presents the first in-situ, non-intrusive, highly detailed measurements of thermochemical states in such a harsh environment. Evaluated temperature profiles indicate the strong influence of biomass particles on the combustion process. Analyses of the O2-T, CO2-T, and O2-CO2 state spaces at different positions are possible with the developed O2-CO2-CARS setup, providing insight into the combustion process and improving our understanding of the physicochemical processes in pulverized oxy-fuel combustion.

CRediT authorship contribution statement

Henrik Schneider: Designed experiment, Performed experiments, Analyzed data, Wrote the paper. **Janik Hebel:** Performed experiments, Discussion of results. **Benjamin Böhm:** Discussion of results. **Reinhold Kneer:** Designed research, Discussion of results. **Andreas Dreizler:** Designed research, Discussion of results.

Declaration of competing interest

The authors declare that they have no known competing financial interests or personal relationships that could have appeared to influence the work reported in this paper.

Acknowledgments

This work was funded by the Deutsche Forschungsgemeinschaft, Germany (Projektnummer 215035359 — TRR 129).

Appendix A. Supplementary data

Supplementary material related to this article can be found online at https://doi.org/10.1016/j.proci.2024.105457.

References

[1] D. Zabrodiec, A. Massmeyer, J. Hees, O. Hatzfeld, R. Kneer, Flow pattern and behavior of 40 kWth pulverized torrefied biomass flames under atmospheric and oxy-fuel conditions, Renew. Sustain. Energy Rev. 138 (2021) 110493.

[2] P.M.J. Hughes, R.J. Lacelle, T. Parameswaran, A comparison of suction pyrometer and CARS derived temperatures in an industrial scale flame, Combust. Sci. Technol. 105 (1–3) (1995) 131–145.

[3] R. Da Corrêa Silva, T. Kangwanpongpan, H.J. Krautz, Flame pattern, temperatures and stability limits of pulverized oxy-coal combustion, Fuel 115 (2014) 507–520.

[4] J. Emmert, H. Schneider, C. Meißner, E. Sidiropoulos, J.I. Hölzer, T. Seeger, B. Böhm, A. Dreizler, S. Wagner, Characterization of temperature distributions in a swirled oxy-fuel coal combustor using tomographic absorption spectroscopy with fluctuation modelling, Appl. Energy Combust. Sci. 6 (2021) 100025.

[5] A.C. Eckbreth, CARS thermometry in practical combustors, Combust. Flame 39 (2) (1980) 133–147.

[6] M. Aldén, S. Wallin, CARS experiments in a full-scale (10 × 10 m) industrial coal furnace, Appl. Opt. 24 (21) (1985) 3434.

[7] E.J. Beiting, Multiplex CARS temperature measurements in a coal-fired MHD environment, Appl. Opt. 25 (10) (1986) 1684.

[8] J.W. Tröger, C. Meißner, T. Seeger, High temperature O2 vibrational CARS thermometry applied to a turbulent oxy–fuel combustion process, J. Raman Spectrosc. 47 (9) (2016) 1149–1156.

[9] C. Meiß ner, H. Schneider, E. Sidiropoulos, J.I. Hölzer, T. Heckmann, B. Böhm, A. Dreizler, T. Seeger, Investigation on wall and gas temperatures inside a swirled oxy-fuel combustion chamber using thermographic phosphors, O2 rotational and vibrational CARS, Fuel 289 (2021) 119787.

[10] F. Mazza, N. Griffioen, L. Castellanos, D. Kliukin, A. Bohlin, High-temperature rotational-vibrational O2-CO2 coherent Raman spectroscopy with ultrabroadband femtosecond laser excitation generated in-situ, Combust. Flame 237 (2022) 111738.

[11] A.D. Cutler, E.C.A. Gallo, L.M.L. Cantu, WIDECARS spectra fitting in a premixed ethylene–air flame, J. Raman Spectrosc. 47 (4) (2016) 416–424.

[12] H. Schneider, M. Bonarens, J. Hebel, H. Hamel, J. Emmert, B. Böhm, S. Wagner, R. Kneer, A. Dreizler, Combined flow, temperature and soot investigation in oxy-fuel biomass combustion under varying oxygen concentrations using laser-optical diagnostics, Fuel 362 (2024) 130771.

[13] D.G. Goodwin, H.K. Moffat, I. Schoegl, R.L. Speth, B.W. Weber, Cantera: An object-oriented software toolkit for chemical kinetics, thermodynamics, and transport processes, 2022.

[14] G.P. Smith, D.M. Golden, M. Frenklach, N.W. Moriarty, B. Eiteneer, M. Goldenberg, C.T. Bowman, R.K. Hanson, S. Song, W.C. Gardiner Jr., V.V. Lissianski, Z. Qin, GRI-Mech 3.0.

[15] R.P. Lucht, Three-laser coherent anti-Stokes Raman scattering measurements of two species, Opt. Lett. 12 (2) (1987) 78–80.

[16] R.P. Lucht, V. Velur-Natarajan, C.D. Carter, K.D. Grinstead, J.R. Gord, P.M. Danehy, G.J. Fiechtner, R.L. Farrow, Dual-pump coherent anti-Stokes Raman scattering temperature and CO concentration measurements, AIAA J. 41 (4) (2003) 679–686.

[17] S. Roy, T.R. Meyer, R.P. Lucht, V.M. Belovich, E. Corporan, J.R. Gord, Temperature and CO2 concentration measurements in the exhaust stream of a liquid-fueled combustor using dual-pump coherent anti-Stokes Raman scattering (CARS) spectroscopy, Combust. Flame 138 (3) (2004) 273–284.

[18] F. Zentgraf, P. Johe, M. Steinhausen, C. Hasse, M. Greifenstein, A.D. Cutler, R.S. Barlow, A. Dreizler, Detailed assessment of the thermochemistry in a side-wall quenching burner by simultaneous quantitative measurement of CO2, CO and temperature using laser diagnostics, Combust. Flame 235 (2022) 111707.

[19] G. Magnotti, A.D. Cutler, G.C. Herring, S.A. Tedder, P.M. Danehy, Saturation and stark broadening effects in dual–pump CARS of N2, O2, and H2, J. Raman Spectrosc. 43 (5) (2012) 611–620.

[20] R.E. Palmer, The CARSFT computer code for calculating coherent anti-Stokes Raman spectra: User and programmer information, 1989.

[21] M. Marrocco, G. Magnotti, A.D. Cutler, Herman–Wallis corrections in dual–pump CARS intensities for combustion temperature and species, J. Raman Spectrosc. 43 (5) (2012) 595–598.

[22] D.E. Jennings, J.W. Brault, The ground state of molecular hydrogen, J. Mol. Spectrosc. 102 (2) (1983) 265–272.

[23] G. Magnotti, A.D. Cutler, P.M. Danehy, Development of a dual-pump coherent anti-Stokes Raman spectroscopy system for measurements in supersonic combustion, Appl. Opt. 52 (20) (2013) 4779–4791.